J. At. Mol. Sci.
doi: 10.4208/jams.030114.052814a

Vol. **5**, No. 3, pp. 217-230
August 2014

Structures, stabilities and electronic properties of MSn_{10} (M=Li, Be, B, Ca)

Yu-Jie Bai[a,*], Kai-Ming Deng[b], Jing-Ling Shao[a], and Ning Xu[a]

[a] *Department of Physics, Yancheng Institute of Technology, Yancheng 224051, China*
[b] *Department of Applied Physics, Nanjing University of Science and Technology, Nanjing 210094, China*

Received 1 March 2014; Accepted (in revised version) 28 May 2014
Published Online 8 August 2014

Abstract. The effect of impurity atoms on structures, stabilities and electronic properties of MSn_{10} (M= Li, Be, B and Ca) clusters have been investigated using the density functional theory based B3LYP method with cc-pVTZ(-PP) basis set. The results show that the location of the impurity atom depends on the interactions of impurity atoms with the host cluster and the size of the impurity atom itself. The stability has been analyzed based on average binding energy, vertical ionization potential, vertical electron affinity, HOMO - LUMO energy gap and embedding energy. Several clusters, such as $BeSn_{10}$, Sn_{10} and $Sn_{10}^{(2-)}$ with enhanced stability have been identified. The stability of $Sn_{10}(C_{3v})$ can be rationalized using the jellium shell model. Molecular orbital analyses reveal that the enhanced stability of $BeSn_{10}$ and $Sn_{10}^{(2-)}$ (D_{4d}) with 42 valence electrons may arise from a crystal-field splitting of the 1G shell and from the closed-shell nature of the π subsystem, which is subjected to the $2(N_\pi+1)^2$ rule with $N_\pi=1$. Both $BeSn_{10}$ and $Sn_{10}^{(2-)}$ clusters can be considered to be aromaticity with 8π electrons, further confirmed by the large nucleus-independent chemical shift values.

PACS: 31.10.+z, 31.15.ae, 31.15.es

Key words: tin cluster, stability, molecular orbital, aromaticity, nucleus-independent chemical shift

1 Introduction

Since the discovery and macroscopic production[1,2] of fullerenes, the questing for novel highly symmetrical and chemically inert cluster is a focus in current research[3-6], which should be very promising potential building blocks for designing new cluster-assembled nanostructured materials. Symmetric binary clusters could be the ideal building blocks

*Corresponding author. *Email address:* byjycit2013@163.com (Y. -J. Bai)

for these advanced materials, since their unique physicochemical properties can be manipulated nearly at will by altering size, shape, and composition[5,7]. Recently, a larger number of experimental and theoretical investigations have been performed on metal-encapsulated E clusters (E= Ge, Sn, and Pb)[4-14]. For examples, the mass spectral characterization of gas-phase Al-doped Pb_n^+ clusters was reported by Neukermans *et al.*[4], and found considerably enhanced stability of $AlPb_{10}^+$. Geometry optimization at the B3LYP/LanL2DZ level of density functional theory reveals that $AlPb_{10}^+$ is a bicapped tetragonal antiprism structure with D_{4d} symmetry, which the Al atom is encapsulated in a highly coordinated central position. The high stability for $AlPb_{10}^+$, which has 21 delocalized orbitals containing 42 valence electrons is attributed to the close-packed geometrical structure and the crystal-field splitting of the high angular momentum spherical molecular orbital levels according to the structural symmetry of the cluster[15,16]. Then Chen *et al.*[6] calculated the electronic structures and stability of cationic $AlPb_{10}^+$ cluster. The enhanced stability of $AlPb_{10}^+$ may arise from the closed-shell nature of the π subsystem according to the electron counting rule, namely, the $2(N_\pi+1)^2$ rule[17] with $N_\pi=1$, which describes the spherical aromaticity. The large nucleus-independent chemical shift (NICS) values[18] indeed demonstrate the high stability of the cationic $AlPb_{10}^+$ cluster. Subsequently, Bhattacharyya *et al.* further demonstrated the extraordinary high stability of $AlPb_{10}^+$ cluster by mass-selected photodissociation study[19].

A few years ago, Lievens and coworkers[10] demonstrated experimentally that the $ZnSn_{10}$ with D_{4d} symmetry system is a species with enhanced stability; even it is less abundant than the $ZnSn_{12}$ in the experimental mass spectra. Subsequently, $ZnSn_{10}$ cluster has been calculated that possessing 42 valence electrons $ZnSn_{10}$ cluster was assigned to be magic cluster with a spherically aromatic character that satisfies the electron counting rule of $2(N_\pi+1)^2$, namely, containing 8 valence π-electrons with $N_\pi=1$[11]. The enhanced stability of the $ZnSn_{10}$ can also be rationalized by its closed crystal field splitting shell. Recently, coinage metal-encapsulated 10-atom E clusters[12] (E= Ge, Sn, and Pb) were investigated by Tai *et. al*, and found that the global minima with D_{4d} structure anions, which possess 42 valence electrons, turned out to be magic clusters. The enhanced stability of these magic clusters can be rationalized by the spherical aromaticity[17]. Then, they sequentially investigated Ge_{10} and Ge_{10}^{2-} clusters[13] and found they also possessed high stabilities. The investigation reveals that each Ge atom is expected to contribute its four valence electrons to the electron shell configuration, and the result of Ge_{10} contains 40 valence electrons, which is consistent with the electron shell configuration of 40 electrons of jellium shell model (JSM)[20]. Adding two excess electrons into the neutral Ge_{10} forming Ge_{10}^{-2} cluster, leads to an unstable system with open electronic shell configuration. However, due to a distortion to D_{4d} symmetry, the 1G-subshell of Ge_{10}^{-2} is splitting into 2P-subshell which results in a very pronounced energy gap (2.92 eV) at the 42 electron occupancy. They both also can consistently be rationalized by using the spherical aromaticity.

Although a number of experimental and theoretical studies have reported the geometric and electronic properties of small doped Sn clusters, most of these works have

been carried out mainly using transition metal atoms as dopant or focusing on their growth behaviors. According to our best knowledge, only a few theoretical investigations on non-transition metal doped tin clusters were reported. Motivated by these above-mentioned phenomena, we set out to carry out a systematic investigation on the clusters MSn_{10} (M= Li, Be, B and Ca). Actually, both geometrical and electronic configurations must be taken into account to design stable clusters, therefore the criteria of choosing different doping elements are based on their size and number of valence electrons, which in fact governs the nature of interaction. We focus our attention to the MSn_{10} (M=Be, Ca) clusters which are iso-electronic structures with above reported stable clusters. Due to the limited size of the empty Sn_{10} cages, the Be atom may be encapsulated inside the Sn_{10} cage, whereas the Ca atom may cap the Sn_{10} cluster outside. The Li and B atom also can be encapsulated inside the Sn_{10} cage, while Li atom can show the effect of a less electron and B atom can show the effect of an additional electron. The objective of this study is to understand the interactions of different atoms with Sn_{10} cluster and how the atomic size and number of valence electrons can influence the geometry, electron configuration, and stability of a binary cluster.

The rest of this paper is arranged as follows. Section 2 describes briefly theoretical methods. In Section 3, we present the results and discussions. Finally, the conclusion is made in Section 4.

2 Computational methods

Quantum chemical computations are carried out using the Gaussian 03[21]. The geometrical, electronic structures and harmonic vibrational frequencies are determined by using the density functional theory (DFT) method with the hybrid B3LYP functional, which involves the Becke three parameter exchange [22] and Lee-Yang-Parr correlation [23] functionals. In order to save time and improve efficiency, the optimization process is divided into two steps: The first step is to optimize all the initial structures with LanL2DZ basis set [24] to obtain the equilibrium geometrical structures; the second step is to further optimize the few most stable isomers obtained from the first step with the larger cc-pVTZ(-PP) basis set. The correlation-consistent cc-pVTZ basis set [25] is used for Li, Be, B and Ca atoms, whereas the energy-adjusted small-core (22 valence electrons for Sn) pseudopotentials (PP) is used for Sn atoms, labeled as cc-pVTZ-PP [26]. The combination of these two basis sets is represented as cc-pVTZ(-PP) in our calculations. Hence, consequent studies of the MSn_{10} clusters (M=Li, Be, B and Ca) and several other lower-lying isomers are carried out only with B3LYP using the cc-pVTZ(-PP) basis set. We set the structures with the lowest energy but no imaginary frequency to be the ground state structures of clusters.

To check the validity of the applied theoretical methodologies, we calculate the bond length of Sn_2 and HOMO - LUMO energy gap of $Sn_{10}^{(2-)}$. From our calculations, the bonding length of 2.80 Å is in line with the experimental value 2.74 Å[11], and the energy

gap of 2.40 eV is close to theory data 2.39 eV[12]. Therefore, our methods reasonably suit to describe the properties of MSn_{10} clusters.

3 Results and discussion

3.1 Structures of the lower-lying isomers of the MSn_{10} clusters

One of the most important things in the cluster study is to determine their ground state equilibrium geometrical structure of clusters. To obtain the lowest energy isomer of MSn_{10}, a large number of initial geometrical configurations were optimized. The ground-state and some metastable structure of the MSn_{10} clusters, together with their symmetry point group are depicted in Fig. 1, respectively. We also give the most stable structures of Sn_{10}, $Sn_{10}^{(2-)}$ clusters in Fig. 1.

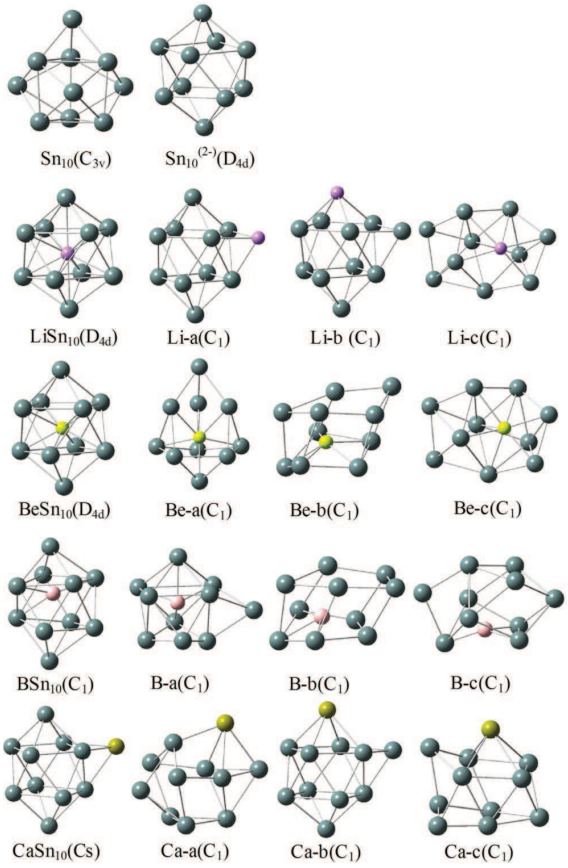

Figure 1: The shape, symmetry point group of ground-state structures of Sn_{10}, $Sn_{10}^{(2-)}$ clusters; ground-state and low-lying structures of MSn_{10} clusters (M= Li, Be, B, Ca).

As for Sn_{10} cluster, tetracapped trigonal prism with C_{3v} symmetry is ground-state

structure, while $Sn_{10}^{(2-)}$ adopts a bicapped tetragonal antiprism structure with D_{4d} symmetry, which are similar to the E_{10} and $E_{10}^{(2-)}$ (E= Ge and Pb) clusters [8, 13]. The ground-state structure of $LiSn_{10}$ can also be viewed as a bicapped tetragonal antiprism structure with D_{4d} symmetry, where the central position is occupied by the Li atom. The distorted bicapped tetragonal antiprism with a face capped by one Li atom (Li-a) is a metastable structure, with 0.19 eV higher in energy than that of the lowest-energy structure. Another isomer structure Li-b is similar to the Li-a, which difference is that Li atom caps the top of the structure with 0.27 eV higher than Li-a structure in energy. All other low-lying isomers of $LiSn_{10}$ are higher than the ground-state structure by at least 1.04 eV in energy. For $BeSn_{10}$, the ground-state structure is similar to the $LiSn_{10}$ cluster with D_{4d} symmetry, which the Be atom is encapsulated in the center. For Be-a is a metastable structure with 0.88 eV higher in energy. A distorted pentagonal prism with a Be atom encapsulated structure Be-b is found as another low-lying structure with 1.29 eV higher in energy above the ground state. All the other structural isomers of $BeSn_{10}$ studied are energetically unfavorable, with more than 1.60 eV energy difference from the ground state. As for BSn_{10}, we find that the distorted bicapped tetragonal antiprism structure with C_1 symmetry encapsulated by a B atom is the most stable structure, which is similar to the $AlPb_{10}$ structure[6]. The metastable structure B-a can be obtained from the ground-state structure, which difference is that one Sn atom caps from side not the bottom. Aonther low-lying structure is distorted pentagonal prism, in which B atom is encapsulated inside. The other considered low-lying isomers, lying more than 0.76 eV energy difference above the most stable state. The lowest-energy structure obtained for $CaSn_{10}$ is a slightly distorted triple capped tetragonal antiprism with Cs symmetry, which a face is capped by the Ca atom. The rest low-lying isomers are also found and they have common character that Ca atoms cap the structures from the outside. At the same time, they show higher energies than the ground state by at least 0.25 eV.

The lowest-energy structures of MSn_{10} (M= Li, Be, B, Ca) clusters are shown in Fig.1. It is seen that, while Li, Be and B atoms get encapsulated inside the Sn_{10} cage, Ca atom favors to cap the triangular face from the outside. The reason for such a different behavior is attributed to the atomic size effect which in turn governs the cage sizes. The atomic radius ratios (M:Sn) of Li, Be ,B and Ca atoms with respect to the Sn atom are calculated to be 1.17, 0.81, 0.68 and 1.30, respectively. It is much difficult for Sn_{10} cage to accommodate a Ca atom since the size of Ca atom is the largest one among the M atoms (Li, Be, B and Ca). Therefore, the appropriate cage volume is required to accommodate the impurity atom. As the size of the impurity atom grows, it will need larger size host cluster to accommodate.

3.2 Stabilities of the ground-state structures MSn_{10} clusters

The relative stability of a cluster can be described by average binding energy (E_b), vertical ionization potential (E_{VIP}), vertical electron affinity (E_{VEA}), HOMO-LUMO energy gap

(E_g) and embedding energy (E_E). In order to probe the inherent stability of clusters, the $E_b, E_g, E_{VIP}, E_{VEA}$ and E_E of the lowest-energy structures of MSn_{10} are given in Table 1.

Table 1: Average binding energy (E_b), vertical ionization potential (E_{VIP}), vertical electron affinity (E_{VEA}), HOMO-LUMO energy gap (Eg) and embedding energy (E_E) of the global minima Sn_{10}, $Sn_{10}^{(2-)}$ and MSn_{10} clusters (M= Li, Be, B, Ca) using the B3LYP/ cc-pVTZ(-PP) level.

Structure	E_b(eV)	Eg(eV)	E_{VIP}(eV)	E_{VEA}(eV)	E_E(eV)
$LiSn_{10}$	3.27	1.05	6.37	2.80	1.62
$BeSn_{10}$	3.43	2.71	6.62	1.36	3.37
$CaSn_{10}$	3.26	1.81	5.84	1.87	1.53
BSn_{10}	3.45	1.15	5.49	1.84	3.59
Sn_{10}	3.44	2.34	6.60	1.77	-
$Sn_{10}^{(2-)}$	3.40	2.40	-	-	-

In the following we have discussed these issues separately to understand the stability of different clusters studied in this work with proper perspective.

The average binding energy (E_b) of pure Sn and M-doped MSn_{10} clusters are defined as follows:

$$E_b = [nE(Sn) + E(M) - E(MSn_n)]n(n+1) \quad \text{for} \quad MSn_n, \tag{1}$$

$$E_b = [nE(Sn) - E(Sn_n)]/n \quad \text{for} \quad Sn_n, \tag{2}$$

$$E_b = [(n-2)E(Sn) + 2E(Sn^{1-}) - E(Sn_n^{2-})]/n \quad \text{for} \quad Sn_n^{2-}. \tag{3}$$

Where $E(Sn)$, $E(M)$, $E(MSn_n)$, $E(Sn_n)$, $E(Sn^{1-})$, $E(Sn_n^{2-})$, and M = Li, Be, B, Ca are the total energies of the atoms or clusters at the neutral and anionic states, respectively.

From Table 1, it can be seen that the BSn_{10} cluster possesses the largest E_b value, being equal to 3.45 eV. The E_b values of $Sn_{10}^{(2-)}$ and $BeSn_{10}$ have 3.40 and 3.43 eV, respectively. Compared to the system containing 42 valence electrons reported earlier, namely E_b ($ZnSn_{10}$)=2.44 eV[11], the isoelectronic species $Sn_{10}^{(2-)}$ and $BeSn_{10}$ are thus characterized by large E_b values that ultimately indicate their higher thermodynamic stability. Furthermore, the neutral Sn_{10} has somewhat higher E_b value than the corresponding dianion, it also possesses relatively higher thermodynamic stability. However, $LiSn_{10}$ and $CaSn_{10}$ clusters have lower E_b values. This is because that even though the $LiSn_{10}$ cluster possesses the same structure D_{4d} symmetry as $Sn_{10}^{(2-)}$ and $BeSn_{10}$, while Li atom has one less electron. And $CaSn_{10}$ even though has 42 valence electrons, whereas it has lower symmetry (Cs). Therefore, $LiSn_{10}$ and $CaSn_{10}$ have lower thermodynamic stability than the other clusters.

Because of the high stability of the endohedral structures MSn_{10}, evaluation of the embedding energy (E_E) is necessary. Embedding energy can be considered as the energy released upon doping M into the Sn_{10} cages, and defined as follows:

$$E_E = E(Sn_{10}) + E(M) - E(MSn_{10}) \tag{4}$$

where $E(Sn_{10})$, $E(M)$ and $E(MSn_{10})$, and M = Li, Be, B, Ca are the total energy of the global minima at the neutral states, respectively.

A high E_E value indicates a strong interaction between M and the host Sn_{10}, and consequently leads to a high thermodynamic stability of the relevant MSn_{10} cluster. In our calculation, all MSn_{10} clusters have the positive E_E values; therefore, the reactions to synthesize them are exothermic [27] and favorable from the energy point of view. The E_E values of the MSn_{10} (M= Be and B) are considerably larger than $CaSn_{10}$. Such remarkably difference can be understood because the former adopt endohedral structures, the latter adopt exohedral structures. Furthermore, the E_E values of the $BeSn_{10}$ and BSn_{10} amount to 3.37 and 3.59 eV, respectively. Those are also remarkably higher than the value of 1.62 eV for $LiSn_{10}$ cluster. Therefore, from the E_E energy point of view, $BeSn_{10}$ and BSn_{10} clusters may be more stable than $LiSn_{10}$ and $CaSn_{10}$ clusters, which accords with the trend of average binding energy.

The HOMO-LUMO energy gap (E_g) is an important electronic property, and is usually considered as a measure of chemical stability of compounds. Generally speaking, the cluster with larger energy gap indicates that the compound is more inert with respect to chemical reactions. As seen from Table 1, the energy gap of $BeSn_{10}$ is equal to 2.71 eV, being the largest gap as compared to those of the other clusters. Compared to the previously reported $ZnSn_{10}$ cluster ($E_g = 2.40$ eV)[11], which leads a further support for its enhanced chemical stability. Furthermore, Sn_{10} and $Sn_{10}^{(2-)}$ also have higher energy gap, 2.34 and 2.40 eV, respectively. However, it is essential to note the energy gaps of the MSn_{10} (M=Li, B, Ca) are remarkably smaller than their host Sn_{10}. The larger energy gap of $BeSn_{10}$, Sn_{10} and $Sn_{10}^{(2-)}$ imply that these clusters are less reactive and have the stronger chemical stability than MSn_{10} (M=Li, B, Ca) clusters.

The vertical ionization potential (E_{VIP}) and vertical electron affinity (E_{VEA}) are also important properties for determining the stability of clusters. The E_{VIP} and E_{VEA} are defined as follows:

$$E_{VIP} = E_n^+ - E_n^- \tag{5}$$

$$E_{VEA} = E_n - E_n^- \tag{6}$$

where E_n^+ and E_n^- are the total energies of ionic clusters at the neutral optimized geometry. From Table 1, it can be seen that the Sn_{10} cluster possess larger E_{VIP} values (6.60 eV), implying it is difficult to remove electrons from these clusters. Furthermore, they possess lower E_{VEA} value (1.77 eV), implying it is not easy to obtain electrons from outside. Whereas, BSn_{10} cluster possesses the lowest E_{VIP} value (5.49 eV) as compared to the other clusters. This means that it is easy to remove electrons from BSn_{10} cluster. For BSn_{10}, having 43 valence electrons, the HOMO energy level is found to occupy by one electron, leaving a large gap between HOMO and HOMO-1. Therefore, it is clear that the one electron occupied HOMO orbital is primarily responsible for the low E_{VIP} of BSn_{10} cluster. From the electronic structure, the large gap between HOMO and HOMO-1 indicates that

the removal of one electron from the HOMO orbital of BSn_{10} would result in a closed shell structure with extra stability. Hence, substitution of the B atom with an appropriate divalent atom could be a good choice to result in a stable cluster. To verify this fact we have calculated the $BeSn_{10}$ cluster. As seen from Table 1, the $BeSn_{10}$ cluster possess larger E_{VIP} values (6.62 eV) and lower E_{VEA} value (1.36 eV), implying it is not easy to obtain or remove electrons and is a stable cluster. The reason for the lowest E_{VIP} value of BSn_{10} cluster may be interpreted that removing one electron, BSn_{10} would possess 42 valence electrons, which is isoelectronic with enhanced stability of $AlPb_{10}^{+}$ and $ZnSn_{10}$ clusters by previous reported experimentally[4, 10]. In addition, the relative higher value of E_{VIP} for $LiSn_{10}$ (6.37 eV) suggests that it also does not facilitate to remove electrons from this cluster. However, it possesses the largest E_{VEA} value (2.80 eV), implying it is easy to obtain electrons from outside. This result agrees well with the lower Eg value for $LiSn_{10}$ cluster. This is because that $LiSn_{10}$ would also possess 42 valence electrons by obtaining one electron, forming a closed shell structure. It is noteworthy that the BSn_{10} cluster possesses the largest E_b and E_E values among these clusters. In contrast to this, the E_{VIP} and Eg of BSn_{10} (5.49 and 1.15 eV, respectively) are found to show smaller values as compared to the other clusters. Therefore, from the energy point of view, the BSn_{10} cluster may be more stable; however its low E_{VIP} and energy gap (Eg) make the cluster electronically unstable or more reactive. Accordingly, BSn_{10} cluster can not be considered as a stable cluster. Therefore, $BeSn_{10}$ and Sn_{10} clusters have more stability than MSn_{10} (M=Li, B, Ca) clusters, in consistence with the above Eg discussion.

As above discussion, considering these several qualities, it is obvious that $BeSn_{10}$, Sn_{10} and $Sn_{10}^{(2-)}$ are more stable than MSn_{10} (M=Li, B, Ca) clusters. The results because that Li atom possesses one less electron than Be atom but B atom can show an additional electron, and Ca atom cannot be encapsulated inside the Sn_{10} cage, owing to it is the largest one among the M atoms (M = Li, Be, B and Ca). Thus, we can conclude that the size and number of valence electrons of the encapsulated atom are important to the geometrical structure and stability of M encapsulated MSn_{10} clusters.

3.3 Electronic structure

As observed from above discussion, Sn_{10} (C_{3v}) and $Sn_{10}^{(2-)}$, $BeSn_{10}$ (D_{4d}) structures are found to possess an enhanced thermodynamic and chemical stability. Apart from above consideration for stability, the detailed analysis of the electronic structure and aromaticity are also important to understand the stability of any species.

3.3.1 Electronic structure of Sn_{10} cluster

In order to probe the stability of Sn_{10} cluster, we examine its molecular orbital (MO) pictures under the viewpoint of the JSM[20], which is applied successfully to interpret the stability motif of different types of atomic clusters. The JSM is based on free electron theory, in which the valence electrons are assumed to be freely itinerant in a simple mean-field potential formed by the nuclei of atoms. The valence electrons fill the spherical

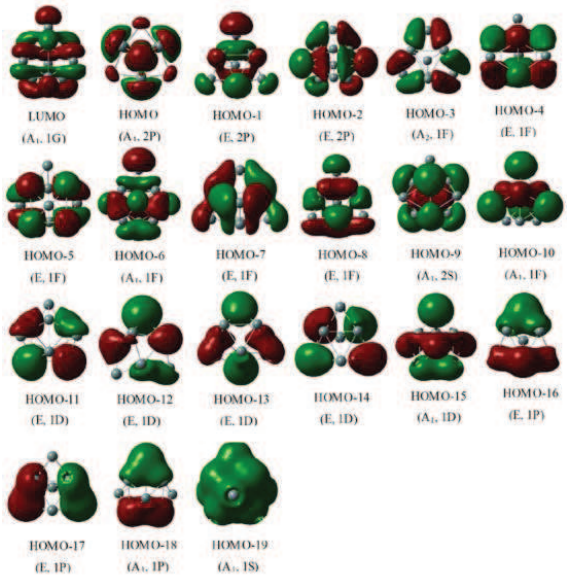

Figure 2: Representation of the 21 frontier molecular orbitals for Sn_{10} (C_{3v}) cluster using the B3LYP/ cc-pVTZ(-PP) level.

orbits of a system according to the pattern of $1S^2 1P^6 1D^{10} 2S^2 1F^{14} 2P^6\ 1G^{18} 2D^{10}$... etc. As a consequence, JSM predicts that higher stability of a magic cluster occurs at the electron shell closure, which corresponds to 8, 20, 34, 40, 58, 68 electrons.

Let us show the MO pictures of Sn_{10} (C_{3v}) in Fig. 2. Each Sn atom is expected to offer four valence electrons to the electron shell configuration of the system. The 20 occupational MOs are occupied by all 40 valence electrons. Because the C_{3v} point group symmetry is lower than a spherical background, the model shells are split into different energy levels, which are ordered according to the C_{3v} splitting. Thus the 40 valence electrons of the Sn_{10} (C_{3v}) are distributed in the following electron configuration: $[1a_1^2 2a_1^2 1e^4 3a_1^2 2e^4 3e^4 4a_1^2 5a_1^2 4e^4 6a_1^2 5e^4 1a_2^2 6e^4 7a_1^2]$. This corresponds to an energy levels sequence of electronic shell model, namely, $[1S^2\ 1P^6\ 1D^{10} 1F^2 2S^2\ 1F^{12}\ 2P^6]$. As shown in Fig. 2, the HOMO of the Sn_{10} is a P-orbit, which is occupied fully. Its LUMO is a G-orbit, belongs to the model G-subshell. This gives rise to a consequence that Sn_{10} possesses a 40 electrons closed electron shell configuration of JSM and thereby has a higher stability, as compared to Ge_{10} cluster [13].

3.3.2 Electronic structure of $Sn_{10}^{(2-)}$ and $BeSn_{10}$ clusters

The 21 MOs occupied by all 42 valence electrons have been exhibited in Fig. 3 for the global minimum $Sn_{10}^{(2-)}$ and $BeSn_{10}$ clusters. As shown in Fig. 3(a), due to a lowering from a spherical background to the D_{4d} point group symmetry, many model shells are split into different subshell levels, such as l =3(1F), 1(2P), 4(1G), and so on. For example,

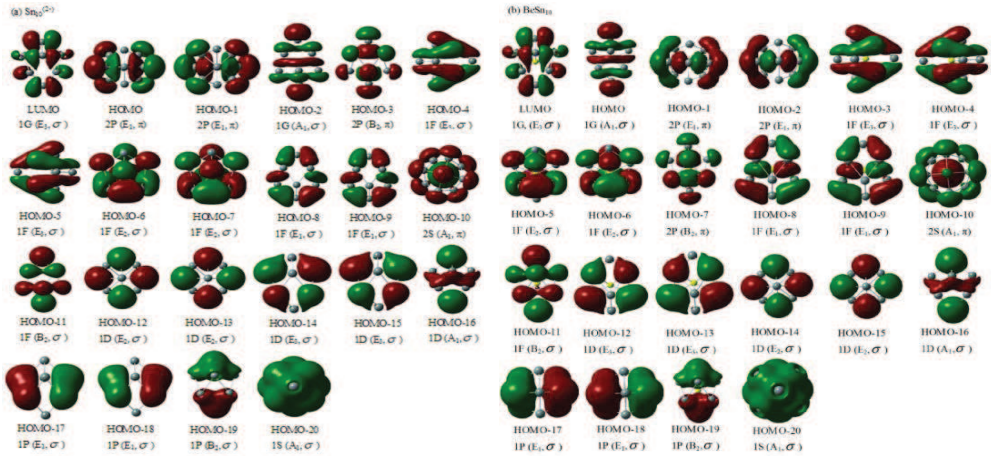

(a) (b)

Figure 3: Representation of the 22 frontier molecular orbitals of the most stable structure of (a) the dianionic $Sn_{10}^{(2-)}$ cluster and (b) the neutral $BeSn_{10}$ cluster using the B3LYP/ cc-pVTZ(-PP) level. The 2P (E_1, π), 2P (B_2, π), and 2S (A_1, π) are cluster π orbitals.

the l =1(2P) shell level splits into two different subshell levels. One is a $2P^2$ type valence MO (B_2 symmetry) holding two electrons; another is double degenerate $2P^4$ type (E_1) subshell. More importantly, long before the first spherical progression is complete; the second set begins and blends into the first: 2S, 2P. Consequently, 34σ valence electrons ($1S^2$+$1P^6$+$1D^{10}$+$1F^{14}$+$1G^2$) which occupy the MOs of 1S (A_1, σ), 1P (B_2, σ), 1P (E_1, σ), 1D (A_1, σ), 1D (E_3, σ), 1D (E_2, σ), 1F (B_2, σ), 1F(E_1, σ), 1F (E_2, σ), 1F (E_3, σ), and 1G (A_1, σ) form the first spherical set and 8π electrons ($2S^2$+$2P^6$) which occupy the 2S (A_1, π), 2P (B_2, π) and the 2P (E_1, π) orbitals form the second set. These (34+8) electrons from two spherical sets constitute the 42 valence electrons of the $Sn_{10}^{(2-)}$ cluster. As shown in Fig. 3(b), the MOs of the $BeSn_{10}$ cluster is similar to that of $Sn_{10}^{(2-)}$ while with some differences from that of $Sn_{10}^{(2-)}$. From the comparison of the 21 frontier occupational MOs of $BeSn_{10}$ and $Sn_{10}^{(2-)}$, we find that although the energetic order of 21 frontier MOs for the $BeSn_{10}$ and $Sn_{10}^{(2-)}$ is different, the overall nature of all the 21 MOs for these two clusters is the same. It can be seen that the 1G (A_1, σ) orbit is the HOMO in the $BeSn_{10}$ cluster while the orbit 2P (E_1, σ) is the HOMO of the $Sn_{10}^{(2-)}$.

Here, we should note that the observed number of electrons of JSM is predicted on the basis of a spherical background. However, symmetry specific deviations could be observed depending on the geometrical features of the cluster structure. Thus, these magic numbers can be changed due to a lowering of the molecular symmetry. This is evident from the previous reported computations, which clearly show that 42 electrons correspond to the electronic magic number systems [4, 6, 11-13]. As a result, the 42 electron closed shell configuration can be interpreted as stemming from the crystal-field splitting

of the high angular momentum (high l) spherical levels according to the structural symmetry of the cluster. As shown in Fig. 3, LUMO orbits are both a G-orbit, belongs to the model 1G-subshell, whereas another G-orbit is HOMO-2 orbit for $Sn_{10}^{(2-)}$ and HOMO orbit for $BeSn_{10}$. Therefore, the 1G shell splitting results in a very pronounced energy gap (2.71 eV for $BeSn_{10}$ and 2.40 eV for $Sn_{10}^{(2-)}$, respectively) at the 42 electrons occupancy. Consequently, the higher stability for $Sn_{10}^{(2-)}$ and $BeSn_{10}$ (42 electrons closed shell configuration) clusters can be explained based on stemming from a crystal-field splitting of the 1G shell, which are similar to $AlPb_{10}^{+}$ and $MgPb_{10}$ clusters [4, 28].

Recently, Hirsch *et al.*[17] have developed another electron counting rule, namely, the $2(N_\pi+1)^2$ rule, to describe the spherical aromaticity, which is proven to be an effective criterion for spherical structures. However, aromaticity of planar structures can be qualitatively probed by using Hckel rule of (4 N+2) valence electrons[29]. In the former counting framework, the π-electron system of an icosahedral fullerene, which surrounds the surface of a sphere, can be approximately considered as a spherical electron gas. The wave functions of this electron gas can be characterized by the angular momentum quantum numbers $(l=0,1,2,3\ldots)$ that are comparable to the atomic s, p, d, f, … orbits, and so forth. According to the classical Pauli principle, if a spherical system bearing $2(N_\pi+1)^2$ π-electrons fully fills all π-shells, it then is stabilized and exhibits an aromatic character. This rule is not only successfully used to explain the aromaticity of organic compounds[17] but also adopted to predict the aromaticity of inorganic cage molecules [30-32].

As shown in Figs. 3(a) and 3(b), among the 21 occupational MOs, the S-type orbit 2S (A_1, π), the P-type 2P (B_2, π), and double degenerate 2P (E_1, π) orbits are occupied with 8π electrons. It is noticeable that the full filling of 2S and 2P orbits with the 8π electrons satisfy the $2(N_\pi+1)^2$ rule $(N_\pi=1)$. This closed-shell nature of π subsystem may explain the stability and spherical aromaticity of $Sn_{10}^{(2-)}$ and $BeSn_{10}$ clusters. However, we should remind that the $2(N_\pi+1)^2$ electron-counting rule alone cannot explain the aromaticity of these molecules. For example, $Si_{12}^{(2-)}$ cluster also has 8π electrons, which is antiaromatic [33]. Therefore, the further confirmed by the calculations of nucleus-independent chemical shifts (NICS) values will be discussed in detail below.

3.3.3 NICS analyses of $Sn_{10}^{(2-)}$ and $BeSn_{10}$ clusters

NICS values are computed at selected point inside or around a molecule. Aromaticity is characterized by a negative NICS value, antiaromaticity by a positive NICS, and nonaromaticity by a value close to zero. Generally, a ghost atom is placed at the center of a spherical geometry to obtain NICS value. However, within our calculations, it is not feasible to place the ghost atom in the center of the D_{4d} $BeSn_{10}$ cluster, owing to an atom at the central site. In view of similar to previous work[5, 6], we adopt the similar way to study the NICS values of the cluster. For $Sn_{10}^{(2-)}$ structure, we can draw a line (*Lab*), which is vertical to line (*L*1-2), as illustrated in Fig. 4. Note that a is *a* fixed site at the

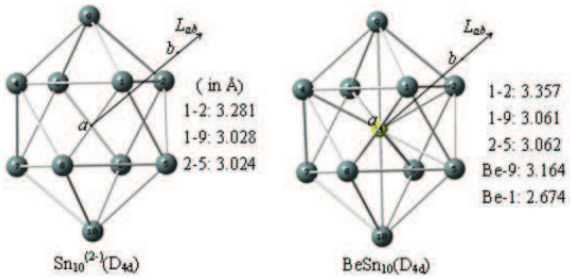

Figure 4: The bond distances of the most stable structures for $Sn_{10}^{(2-)}$ and $BeSn_{10}$ (D_{4d}). Site a is at the center of geometry, and site b is on the line (Lab) that is vertical to bond 1-2. The bond distances are in angstroms.

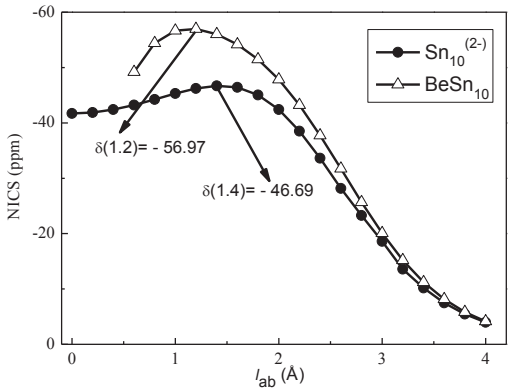

Figure 5: NICS values of the dianionic $Sn_{10}^{(2-)}$ and the neutral $BeSn_{10}$ clusters are represented by solid dots and hollow triangles, respectively.

center of the cage and b is a varying site upon line (Lab). The ghost atom is placed on the line (Lab). The values of NICS for the $Sn_{10}^{(2-)}$ cluster at different sites ($0 \leq lab \leq 4.0$ Å) on Lab are shown in Fig. 5. Finally, adopting the same method we also calculate the NICS values for the $BeSn_{10}$ cluster with $0.6 \leq lab \leq 4.0$ Å as illustrated in Fig. 5. Note that the reported NICS value at the cage center of bare $Sn_{10}^{(2-)}$ (D_{4d}) is -32.10 ppm with B3LYP method using LanL2DZ basis set [34], which is much smaller than the value of -41.69 ppm for the $Sn_{10}^{(2-)}$ with B3LYP/ cc-pVTZ(-PP) level. The remarkable difference shows that it is necessary to use large basis set in our calculations in order to get a proper description of the aromaticity properties.

As shown in Fig. 5, the absolute NICS value [$\delta(0) = -41.69$ ppm] at the center of $Sn_{10}^{(2-)}$ is smaller than those at the sites around, and the absolute $\delta(1.4)$ value at the site ($lab = 1.4$ Å) is the largest. The absolute NICS value increases slowly ($0 \leq lab \leq 1.4$ Å) and reaches its maximum around the site ($lab = 1.4$ Å), then it drops off rapidly when the site is outside of the cage ($lab \geq 2.0$ Å). As to the neutral $BeSn_{10}$ cluster, the absolute δ values at different sites within $0.6 \leq lab \leq 4.0$ Å are also presented in Fig. 5. The absolute δ value at the

site ($lab = 1.2$ Å) is the largest. The magic electronic character for both the $Sn_{10}^{(2-)}$ and the $BeSn_{10}$ clusters is confirmed by the large values of NICS, -46.69 ppm at the site ($lab = 1.4$ Å) for $Sn_{10}^{(2-)}$ and -56.97 ppm at the site (lab=1.2 Å) for $BeSn_{10}$, respectively, revealing that both two clusters exhibit aromatic character and high stabilities. The aromatic character of the $Sn_{10}^{(2-)}$ and its big cavity and electronic structure that host a Be atom efficiently, support the description of the $BeSn_{10}$ as magic clusters.

4 Conclusions

In summary, we have calculated the ground state geometrical structures of MSn_{10} (M = Li, Be, B and Ca) clusters. The results reveal that the atomic size and number of valence electrons of the impurity atom play the crucial role to determine the structure and stability of the system. An optimum cage diameter of the host cluster is required to encapsulate the specific size and electronic configurations of impurity atom. The higher stability of $BeSn_{10}$, Sn_{10} and $Sn_{10}^{(2-)}$ clusters were analyzed based on the average binding energy, embedding energy, HOMO - LUMO energy gap and vertical ionization potential, vertical electron affinity. At the same time, the MO analyses show that (1) the enhanced stability of Sn_{10} can consistently be rationalized by using the jellium shell model; (2) the higher stability for $Sn_{10}^{(2-)}$ and $BeSn_{10}$ clusters can be interpreted by the crystal-field splitting of the high angular momentum (high $l = 4$) spherical levels according to the structural symmetry of the cluster; (3) 8π electrons of $BeSn_{10}$ and $Sn_{10}^{(2-)}$ clusters comply with the spherical aromaticity $2(N_\pi+1)^2$ rule $(N_\pi = 1)$, reflecting the closed-shell nature of π subsystem. The magic character of $BeSn_{10}$ and $Sn_{10}^{(2-)}$ are further confirmed by the large NICS value[$\delta(1.4) = -46.69$ ppm for $Sn_{10}^{(2-)}$ and $\delta(1.2) = -56.97$ ppm for $BeSn_{10}$], indicating the aromatic character. In conclusion, the higher stability is due to the combined effect of highly symmetric close-packed structures, closed crystal-field split electron shell configurations, and a three-dimensional aromatic character. These species should be very promising potential building blocks for cluster-assembled nanostructured materials.

Acknowledgments. Project is supported by the National Natural Science Foundation of China (Grant Nos. 11204265 and 11204266) and the Natural Science Foundation of the Higher Education Institutions of Jiangsu Province (Grant No. 13KJB140018).

References

[1] H. W. Kroto, J. R. Heath, S. C. O'Brien, R. F. Curl, and R. E. Smalley, Nature 318 (1985) 162.
[2] W. Krátschmer, L. D. Lamb, K. Fostiropoulos, and D. R. Huffman, Nature 347 (1990) 354.
[3] J. Li, X. Li, H. J. Zhai, and L. S. Wang, Science 299 (2003) 864.
[4] S. Neukermans, E, Janssens, Z. F. Chen, R. E. Silverans, P. V. R. Schleyer, and P. Lievens, Phys. Rev. Lett. 92 (2004) 163401.
[5] D. L. Chen, W. Q. Tian, W. C. Lu, and C. C. Sun, J. Chem. Phys. 124 (2006) 154313.

[6] D. L. Chen, W. Q. Tian, and C. C. Sun, Phys. Rev. A 75 (2007) 013201.
[7] V. Kumar and Y. Kawazoe, Phys. Rev. Lett. 88 (2002) 235504.
[8] Y. J. Bai, H. Y. Cheng, H. Q. Sun, N. Xu, and K. M. Deng, Phys. B 406 (2011) 3781.
[9] X. Chen, K. M. Deng, Y. Z. Liu, C. M. Tang, Y. B. Yuan, W. S. Tan, and X. Wang, J. Chem. Phys. 129 (2008) 094301.
[10] S. Neukermans, X. Wang, N. Veldeman, E. Janssens, R. E. Silverans, and P. Lievens, Int. J. Mass. Spectrosc. 252 (2006) 145.
[11] T. B. Tai, N. M. Tam, and M. T. Nguyen, Chem. Phys. 388 (2011) 1.
[12] T. B. Tai and M. T. Nguyen, J. Phys. Chem. A 115 (2011) 9993.
[13] T. B. Tai and M. T. Nguyen, J. Chem. Theor. Comput. 7 (2011) 1119.
[14] V. Kumar, A. K. Singh, and Y. Kawazoe, Nano Lett. 4 (2004) 677.
[15] H. P. Cheng, R. S. Berry, and R. L. Whetten, Phys. Rev. B 43 (1991) 10647.
[16] K. E. Schriver, J. L. Persson, E. C. Honea, and R. L. Whetten, Phys. Rev. Lett. 64 (1990) 2539.
[17] A. Hirsch, Z. F. Chen, and H. J. Jiao, Angew. Chem. Int. Ed. 39 (2000) 3915, A. Hirsch, Z. F. Chen, and H. J. Jiao, Angew. Chem. Int. Ed. 40 (2001) 2834.
[18] P. V. R. Schleyer, C. Maerker, A. Dransfeld, H. Jiao, and N. J. R. Van, J. Am. Chem. Soc. 118 (1996) 6317.
[19] S. Bhattacharyya, T. T. Nguyen, J. D. Haeck, K. Hansen, P. Lievens, and E. Janssens, Phys. Rev. B 87 (2013) 054103.
[20] M. Brack, Rev. Mod. Phys. 65 (1993) 677.
[21] M. J. Frisch, G. W. Trucks, H. B. Schlegel, *et al.*, Gaussian 03 (Gaussian, Inc., Pittsburgh, PA, 2003).
[22] A. D. Becke, J. Chem. Phys. 98 (1993) 5648.
[23] C. Lee, W. Yang, and R. G. Parr, Phys. Rev. B 37 (1988) 785.
[24] P. J. Hay and W. R. Wadt, J. Chem. Phys. 82 (1985) 270.
[25] T. H. J. Dunning, J. Phys. Chem. A 106 (2002) 9595.
[26] K. A. Peterson, J. Chem. Phys. 119 (2003) 11099.
[27] P. Kuran, M. Krause, A. Bartl, and L. Dunsch, Chem. Phys. Lett. 292 (1998) 580.
[28] C. Rajesh and C. Majumder, J. Chem. Phys. 128 (2008) 024308.
[29] A. I. Boldyrev and L. S. Wang, Chem. Rev. 105 (2005) 3716.
[30] Z. Chen, A. Hirsch, S. Nagase, W. Thiel, and P. V. R. Schleyer, J. Am. Chem. Soc. 125 (2003) 15507.
[31] M. P. Johansson, D. Sundholm, and J. Vaara, Angew. Chem. Int. Ed. 43 (2004) 2678.
[32] J. Wang, J. Jellinek, J. Zhao, Z. Chen, R. B. King, and P. V. R. Schleyer, J. Phys. Chem. A 109 (2005) 9265.
[33] R. B. King, T. Heine, C. Corminboeuf, and P. V. R. Schleyer, J. Am. Chem. Soc. 126 (2004) 430.
[34] Z. F. Chen, S. Neukermans, X. Wang, E. Janssens, Z. Zhou, R. E. Silverans, R. B. King, P. R. Schleyer, and P. Lievens, J. Am. Chem. Soc. 128 (2006) 12829.